Inorganic Chemistry

Article

pubs.acs.org/IC

Chelate Ring Size Effect as a Factor of Selective Fluorescent Recognition of Zn^{2+} Ions by Pyrrolo[2,3-*b*]quinoxaline with a Substituted 2-Pyridyl Group Receptor

Katarzyna Ostrowska,* Bogdan Musielak, Edward Szneler, Łukasz Dudek, Marlena Gryl, and Katarzyna Stadnicka†

*Department of Organic Chemistry, Jagiellonian University, R. Ingardena 3, PL-30060 Kraków, Poland

Supporting Information

ABSTRACT: Analysis of the spectral properties and structural differences of two turn-on ratiometric fluorescent receptors for Zn^{2+} and Cd^{2+} ions, derivatives of pyrrolo[2,3-*b*]quinoxaline (**2**), and earlier published **3** (Ostrowska et al. *CrystEngComm* **2015**, *17*, 498−502) was performed. Both ligands are *E*/*Z* push−pull olefins interconverting at room temperature, with barriers to rotation about enamine double bonds, from *E* to *Z* isomers of 19.3 ± 0.1 and 16.9 ± 0.3 kcal/mol and from *Z* to *E* of 16.9 ± 0.3 and 15.7 ± 0.2 kcal/mol, respectively. Diastereoisomers (*E*)-**2** and (*Z*)-**2** were isolated and characterized by X-ray structural analysis. The formation of complexes by (*E*/*Z*)-**2** with acetates and acetylacetonates of Zn^{2+} and Cd^{2+} was monitored by UV−vis, fluorescence, and ^{1}H NMR titrations in acetonitrile, respectively. X-ray structural analysis for isolated [(*E*)-**2**]$_2$Zn in relation to earlier published (*E*)-**3**-ZnOAc revealed the formation of a six-coordinated zinc ion with six- and four-membered bis-chelate rings by (*E*)-**2**. The chelate effect increases the ligand affinity for Zn^{2+} (log β_{12} = 12.45) and causes the elongation of nitrogen−metal bonds. Extension of the coordination cavity size allows coordination of a cadmium ion. The introduction of a flexible ethylene linker between the fluorophore and ionophore pyridyl groups in **3** significantly affects the selectivity of zinc-ion recognition. The distorted tetrahedral geometry of (*E*)-**3**-ZnOAc with a four-coordinated zinc ion appears to be the most preferred because of the short donor−zinc distance with a 1:1 binding mode. The formation of the small coordination cavity size with six-membered bis-chelate rings provides an effective overlap of zinc and donor orbitals, precluding the coordination of a cadmium ion in the same manner as zinc.

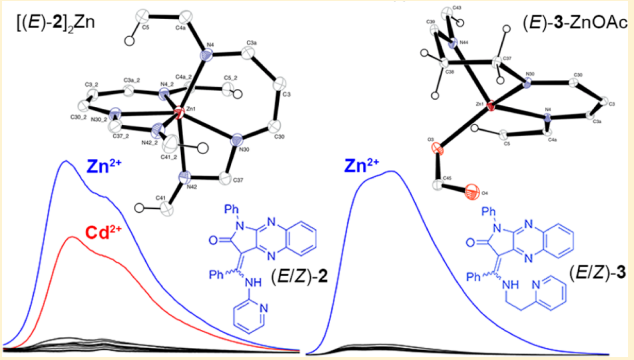

INTRODUCTION

Zinc metal ions are involved in essential life processes, are included as a component of over 200 enzymes that regulate the metabolism of carbohydrates, lipids, proteins, and nucleic acids, and are responsible for the inhibition of inflammation. Deficiency or excess of zinc influences the immune system and is connected to a variety of health problems, including neuronal and sensory dysfunctions such as Alzheimer's or Parkinson's diseases, epilepsy, and amyotrophic lateral sclerosis.[1−3] Bioimaging and biodistribution of Zn^{2+} in cells helps explain the origins of various diseases. The monitoring of zinc ions is possible due to selective fluorescent sensors, which change their photophysical properties upon binding the metal ions.[4,5] The enhancement of the fluorescence intensity during metal chelation (the CHEF effect) at a specific emission wavelength corresponds to the concentration of the metal ion. The concentration of zinc ions ranges from the picomolar scale for "mobile" zinc in cells to 10 μM in serum and 300 μM in neuronal cells in the brain.[6]

There are two main mechanisms of photophysical signal transduction that can be used to design sensors that exhibit changes in fluorescence in response to zinc ions: photoinduced electron transfer (PET) and internal charge transfer (ICT).[7] Both mechanisms are based on electron transfer in a system with a donor−acceptor architecture. For PET-based sensors, the fluorescence of the ligand is quenched due to electron transfer from the donor atoms, usually nitrogen atoms, to the acceptor fragment, usually a π-system separated from the donor group by an alkylene spacer. During binding, metal ions produce a strong electrostatic attraction to the pair of these electrons from the donor fragment, preventing their transfer to the acceptor π-system. Engagement of the lone pair of electrons during the formation of metal−nitrogen bonds lessens the quenching and recovers the fluorescence enhancement of a ligand. ICT-based sensors possess a π-conjugated donor−acceptor system with the electron-withdrawing and electron-donating groups located on opposite sides, which induces polarization of the molecule. Coordination of Zn^{2+} alters the photoinduced ICT of the excited sensor state. Formation of the

Received: May 18, 2015
Published: August 20, 2015

DOI: 10.1021/acs.inorgchem.5b01533
Inorg. Chem. 2015, 54, 8423−8435

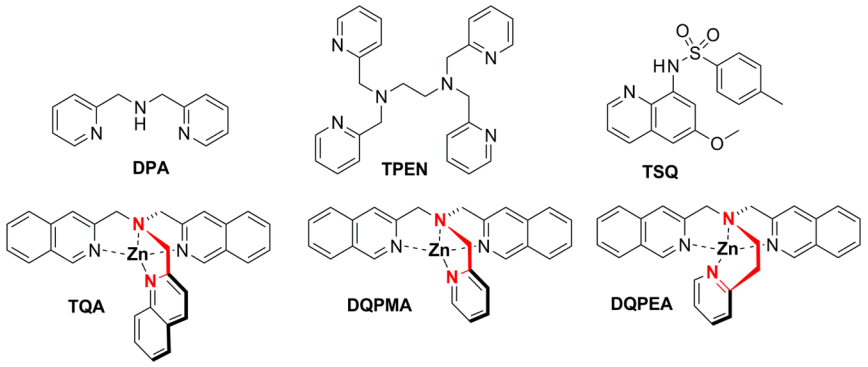

Figure 1. Fluorescent ligands and complexes of zinc with pyridyl- and quinolyl-based groups.

complex with zinc results in the reduction or extension of the π-conjugated system. Interaction of metal ions with the donor groups leads to the reduction of the conjugation and to the occurrence of a blue shift in the UV−vis spectra. In contrast, the interaction of zinc ions with the acceptor groups extends the conjugation, resulting in a red shift in the UV−vis spectra.

The widely used design of PET or ICT fluorescent chemosensors for zinc ion recognition is the receptor−fluorophore approach. Receptor groups with nitrogen donors coordinate metal ions by forming five- or six-membered chelate rings with binding modes of 1:1 or 1:2. The number of nitrogen donors and the geometry of the ionophore moieties influence the formation of a tetrahedral, trigonal-bipyramidal, square-pyramidal, or octahedral geometry of the complex.[5] Fluorescence enhancement upon chelation of zinc ions is controlled by several factors including a small spin−orbit coupling constant, the ionic charge, and steric effects. Steric effects are highly dependent on the relationship between the ligand geometry and the metal-ion radius, which for zinc ions increases with the coordination number (given in parentheses): 0.60 Å (4), 0.68 Å (5), and 0.74 Å (6).[8] The size of the metal ion controls the stability of the five- and six-membered chelate rings formed during receptor binding. Zinc ions fit the size of the six-membered chelate rings with small bite angles better to form short zinc−nitrogen bonds that are strongly involved in the efficient overlap of the donor orbital with the metal ions. The six-membered chelate ring coordinates zinc with a minimum strain in binding to the nitrogen donors through an interaction intermediate between the closed and shared shells (both ionic and covalent contributions to the bonding). Five-membered chelate rings are preferred for metal ions with larger ionic radii than that of zinc.[9]

The most common receptors (Figure 1) to construct Zn^{2+} chemosensors are pyridyl and quinolyl donor groups, especially in bis(2-pyridylmethyl)amine (DPA),[10−13] *N*,*N*,*N*′,*N*′-tetrakis-(2-pyridylmethyl)ethylenediamine (TPEN), tris(2-quinolylmethyl)amine (TQA),[14] *N*,*N*,*N*′,*N*′-tetrakis(2-quinolylmethyl)ethylenediamine (TQEN),[15] *N*,*N*-bis(2-quinolylmethyl)(2-pyridylmethyl)amine (DQPMA),[16] or *N*,*N*-bis(2-quinolylmethyl)-2-(2-aminoethyl)pyridine (DQPEA)[16] and 8-arylsufonamidoquinoline derivatives (TSQ, Zinquin).[17,18] DPA, DPEN, TRPEN, and TSQ coordinate zinc ions through the formation of five-membered chelate rings in a trigonal-bipyramidal or octahedral geometry, and they are therefore susceptible to interference by metals with the same electronic configuration[19] and a larger ionic radius (e.g., Cd^{2+} and Hg^{2+}). The expansion of the chelate ring size from five-membered in DQPMA to six-membered in DQPEA produces an increase in the selectivity for Zn^{2+} over Cd^{2+}.[16]

We previously designed selective ICT ratiometric fluorescent receptors for zinc ions based on the *E*/*Z* diastereoisomers of *N*-arylpyrrolo[2,3-*b*]quinoxaline or pyrido[2,3-*b*]pyrrolo[2,3-*e*]-pyrazine integrated with an amino alcohol, diaminoalkane, or 2-(2-aminoethyl)pyridine.[20−22] The fluorophore has a donor−acceptor architecture with an electron-donating enamino group and an electron-withdrawing amide moiety. When the metal ion is bound to an electron-donating enamino group, the complexation is associated with isomerization of the *Z* to *E* form and deprotonation of the enamine, inducing rigidity and planarization of the molecule and leading to an enhanced ICT process from the donor to the acceptor upon excitation by light. The replacement of hydrogen by zinc ions and the formation of a six-membered chelate ring broaden the conjugation of the π-system, resulting in a Stokes red shift of the absorption spectra. Our study shows that the distinct fluorescence enhancement and affinity for zinc ions come from ligands containing conjugated nitrogen donors that form six-membered chelate rings with a binding mode of 2:1 or 1:1. The introduction of (3-aminopropyl)amino,[20] (3-hydroxypropyl)-amino,[21] or 2-(2-aminoethyl)pyridyl[22] groups into a fluorogenic component provides an additional metal coordination side. The application of metal acetylacetonate salts with two oxygen donors enables the formation or reorganization of the complex $[(E\text{-L})]_2$Zn to (*E*)-L-Znacac. We evaluated the deprotonation, the conversion of diastereoisomers *Z* to *E*, and the progress of complex formation via ^{1}H NMR titration of the ligands in acetonitrile.

Until now, little has been published on the selectivity of sp^2-hybridized nitrogen pyridyl donor ligands in relation to the zinc ion preference for six-membered chelate ring formation.[14,16,19] In this paper, we demonstrate that the introduction of an ethylene spacer in **3** alters the photophysical properties and changes the coordination cavity size for Zn^{2+} and Cd^{3+} compared with conjugated **2**.

EXPERIMENTAL SECTION

Materials and Methods. All of the solvents for the UV and fluorescence spectra were obtained from Sigma-Aldrich or Merck and were of spectroscopic purity. The solutions of metal salts were prepared from $Zn(acac)_2$, $Zn(OAc)_2$, $Cu(acac)_2$, $Ni(acac)_2$, $Co(acac)_2$, $Cd(acac)_2$, $Cd(OAc)_2$, $Hg(OAc)_2$, NaOAc, $Pb(OAc)_2$, and $Mg(OAc)_2$. Melting points were determined on a Boetius PHMK 05 melting point apparatus. IR spectra were measured on a Thermo Scientific Nicolet IR200 Fourier transform infrared spectrometer. The ^{1}H and ^{13}C NMR spectra were recorded with a Bruker Avance III 600 and Bruker Avance II 300 at 300 K. The chemical shifts (δ) are

DOI: 10.1021/acs.inorgchem.5b01533
Inorg. Chem. 2015, 54, 8423−8435

reported in parts per million (ppm) on a δ scale downfield from tetramethylsilane. The ^{1}H NMR spectra were referenced internally to the residual proton resonance in $CDCl_3$ (δ 7.26 ppm), dimethyl sulfoxide (DMSO-d_6) (δ 2.49 ppm), CD_3CN (δ 1.96 ppm), and MeOD (δ 3.30 ppm). The ^{13}C NMR spectra were referenced to $CDCl_3$ (δ 77.0 ppm) or DMSO-d_6 (δ 39.7 ppm). The coupling constants (J) are reported in hertz (Hz). Mass spectra were measured on Finnigan Mat 95 electron impact (EI, 70 eV) and electrospray ionization (ESI) spectrometers. Microanalyses were performed with a Vario Micro Tube CHNS; the results agreed with the calculated values.

The UV−vis spectra for compounds **2**, **3**, [(*E*)-**2**]$_2$Zn, and (*E*)-**3**-ZnOAc were recorded with a Hitachi U-3900H spectrophotometer in 1 cm cells at 25 °C after equilibration for 20 min.

The fluorescence measurements for **2**, **3**, [(*E*)-**2**]$_2$Zn, and (*E*)-**3**-ZnOAc were carried out using a Hitachi F-4500 spectrofluorometer. All spectra were recorded at 25 °C with an excitation slit width of 5 nm, an emission slit of 5 nm, and 400 or 600 V of photomultiplier tube voltage after equilibration for 20 min.

Molecular Structure Determination. *Crystal Structure Analysis of [(E)-2]$_2$Zn, (Z)-2, and (E)-2.* The single-crystal X-ray diffraction experiment was carried out with an Agilent Technologies SuperNova diffractometer equipped with an Atlas CCD detector using graphite-monochromated Cu Kα or Mo Kα radiation (λ = 1.54178 or 0.71073 Å, respectively). The experimental data were processed with *CrysAlisPro*.[23] Crystallographic data and the details of data collection and crystal structure refinement are summarized in the Supporting Information (Table 1). The structure was solved by direct methods with *SIR92*.[24] A refinement procedure by full-matrix least-squares methods based on F^2 values against unique reflections, including all atomic fractional coordinates and anisotropic displacement parameters for non-hydrogen atoms, was performed with *SHELXL97*.[25] Hydrogen atoms were found from Fourier difference maps and included in the refinement procedure in the riding model assuming isotropic displacement parameters. CCDC 1401449 for [(*E*)-**2**]$_2$Zn, CCDC 1401450 for (*Z*)-**2**, and CCDC 1401451 for (*E*)-**2** contain the supplementary crystallographic data for this paper. These data can be obtained free of charge from the Cambridge Crystallographic Data Centre at www.ccdc.cam.ac.uk/data_request/cif. Molecular graphics were prepared with *ORTEP3*.[26] All programs mentioned above were operated under the *WinGX*[27] program package.

Synthesis. The ligand **3** and (*E*)-**3**-ZnOAc were synthesized using previously published procedures.[22]

Synthesis of (E/Z)-3-[(Pyridin-2-ylamino)phenylmethylidene]-1,3-dihydro-2H-1-phenylpyrrolo[2,3-b]quinoxalin-2-one (2). 1-Phenyl-1,4-dihydro-2*H*-3-thiobenzoylpyrrolo[2,3-*b*]quinoxalin-2-one (**1**; 0.5 g, 1.31 mmol) was added to 2-aminopyridine (1.5 g) in *n*-propanol (15 mL). The reaction mixture was heated at 50 °C for 5 days. The precipitated solid was collected by filtration, washed with H_2O, and crystallized from acetonitrile to obtain yellow needles. Yield: 0.215 g, 37.2%. Mp: 248−250 °C for (*E*)-**2** and 237−238 °C for (*Z*)-**2**. IR (KBr): 3049, 1701, 1609, 1561 cm^{-1}. ^{1}H NMR (600.204 MHz, CD_3CN): δ 12.44 (s, 1H, (*E*)-NH), 12.10 (s, 1H, (*Z*)-NH), 8.36 (dd, J = 4.9 and 1.0 Hz, 1H, (*E*)-H-6′), 8.30 (d, J = 5.0 Hz, 1H, (*Z*)-H-6′), 8.01 (m, 1H, (*E*)-H-5), 7.77 (m,1H, (*E*)-H-8), 7.68−7.37 (m, 24H, (*E*/*Z*)-Ar-H), 7.09 (ddd, J = 7.4, 4.9, and 0.9 Hz, 1H, (*E*)-H-5′), 7.05 (dd, J = 7.4 and 4.8 Hz, 1H, (*Z*)-H-5′), 6.39 (d, J = 8.3 Hz, 2H, (*E*/*Z*)-H-3′). ^{13}C NMR (75.47 MHz, DMSO-d_6): δ 168.9, 165.2, 159.3, 159.2, 151.5, 151.3, 149.1, 147.6, 146.4, 144.9, 142.6, 139.6, 138.9, 138.5, 138.3, 133.4. 133.13, 131.1, 131.0, 130.9, 130.7, 129.4, 129.2, 129.2, 129.0, 128.8, 128.7, 128.3, 128.2, 128.1, 127.8, 127.8, 127.7, 127.6, 127.4, 126.9, 126.6, 121.0, 120.8, 116.1, 115.8, 94.6, 94.3. MS-ESI: m/z 442 (M^+ + 1). Anal. Calcd for $C_{28}H_{19}N_5O$: C, 76.18; H, 4.34; N, 15.86. Found: C, 75.83; H, 4.39; N, 15.79.

Synthesis of Complex [(E)-2]$_2$Zn. Zn(OAc)$_2$ (44 mg, 0.24 mmol) was added to a solution of ligand **2** (0.105 g, 0.24 mmol) in anhydrous methanol (MeOH; 3 mL), and the mixture was refluxed for 5 min. The reaction mixture was then allowed to cool to room temperature. The product precipitated from the reaction mixture as a yellow powder was then collected, washed with H_2O, and crystallized from acetonitrile. Yield: 43 mg, 38%. Mp: 325 °C. IR: 3062, 3026, 1698, 1567, 1533 cm^{-1}. ^{1}H NMR (300.13 MHz, DMSO-d_6): δ 7.04 (ddd, J = 4.8, 1.8, and 0.9 Hz, 2H, H-6′), 6.81 (m, 2H, H-5), 6.64 (m, 2H, H-8), 6.56−6.28 (m, 20H, Ar−H), 6.17 (ddd, J = 8.2, 7.3, and 1.8 Hz, 2H, H-4′), 5.76 (ddd, J = 7.3, 4.8, and 0.9 Hz, 2H, H-5′), 4.79 (d, J = 8.2 Hz, 2H, H-3′). ^{13}C NMR (75.47 MHz, DMSO-d_6): δ 169.8, 166.5, 158.4, 147.9, 147.8, 147. 6, 144.9, 144.8, 143.1, 138.2, 137.8, 136.0, 135.6, 133.8, 129.7, 129.5, 129. 3, 129.1, 128.9, 128.8, 128.2, 128.0, 127.8, 127.7, 127.7, 127.5, 126.8, 123.3, 122.2, 120.3, 116.9, 92.8. MS-ESI: m/z 945 (M^+ + 1). Anal. Calcd for $C_{56}H_{36}N_{10}O_2Zn$: C, 71.07; H, 3.83; N, 14.80. Found: C, 69.62; H, 3.82; N, 14.43.

Formation Constant Determination. The analyzed ligand **2** was dissolved in acetonitrile to prepare 0.4 mM and 10 μM stock solutions for the determination of association constants with Zn^{2+} and Cd^{2+} metal ions by monitoring the intense $\pi \rightarrow \pi^*$ transitions in the UV spectra. The 0.1 mM, 0.2 mM, and 25 μM acetonitrile solutions of $Zn(OAc)_2 \cdot 2H_2O$ and $Cd(OAc)_2 \cdot 2H_2O$ were prepared from 10 mM stock solutions of metal salts in DMSO, respectively. The association constants were determined using two methods: titrating the 10 μM solution of **2** with 0.1 M solutions of metal ions and titrating the 25 μM solution of metal salts with 0.4 mM solutions of **2** (0−2.4 equiv of **2** for the Cd^{2+} solution and 0−3.12 equiv of **2** for the Zn^{2+} solution). The titrations were carried out after equilibration for 20 min. The UV−vis titration data at λ = 450 nm obtained during the titration of ligand solutions with metal ions were fitted to the kinetic equation of the 2:1 binding equilibria using a nonlinear regression method.[28] The determined association constants, K_1 = 2.5938 × 10^6 ± 17561.7 M^{-1} and K_2 = 2.56197 × 10^6 ± 16992.9 M^{-1} for complex formation of **2** with Zn^{2+} or K_1 = 1.02928 × 10^7 ± 24913.6 M^{-1} and K_2 = 1.06992 × 10^6 ± 22365.2 M^{-1} for complex formation of **2** with Cd^{2+}, were entered as estimated parameters in analyses of the UV−vis titration data using *ReactLab Equilibria*.[29] The data were obtained during the titration of metal salt solutions with ligand, and plots were fitted to the models M + L = ML, ML + L = ML2. The concentration profiles for the metal salts, ligand **2**, and complexes LM and L$_2$M, the molar absorption spectra, and plots of the measured and fitted data are shown in the Supporting Information.

RESULTS AND DISCUSSION

Synthesis of Ligands, Complex, and ^{1}H NMR Studies. 2-Pyridyl derivatives **2** and **3**[22] were synthesized by the enamination of 3-thiobenzoylpyrrolo[2,3-*b*]quinoxaline **1** with excess 2-amino- and 2-(ethylamino)pyridine in *n*-propanol (Scheme 1). The reactions were carried out at room temperature except for the 2-aminopyridyl derivative **2**, which was heated at 50 °C for 5 days.

Scheme 1. Synthesis of *E*/*Z* Diastereoisomers 2 and 3[22]

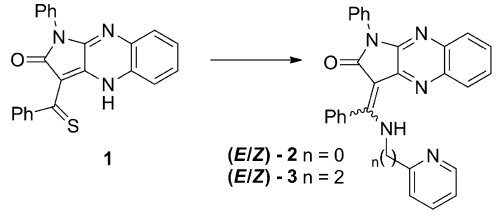

The ^{1}H NMR data showed that, in all cases, we obtained mixtures of the *E*/*Z* diastereoisomers, with the *E* form predominant in DMSO-d_6, CD_3CN, and CD_3OD in molar ratios of 3.34:1, 3.69:1, and 10.61:1 for **2** and 4.07:1, 4.13:1, and 8.53:1 for **3**, respectively[22] (Figure 2). In (*E*/*Z*)-**2** and (*E*/*Z*)-**3**, the enamine NH protons form hydrogen-bonded six-membered rings with either the oxygen of the carbonyl groups or nitrogen N4 of the quinoxaline moiety for the *Z* and *E* forms, respectively. Signals with the diagnostic coupling

DOI: 10.1021/acs.inorgchem.5b01533
Inorg. Chem. 2015, 54, 8423−8435

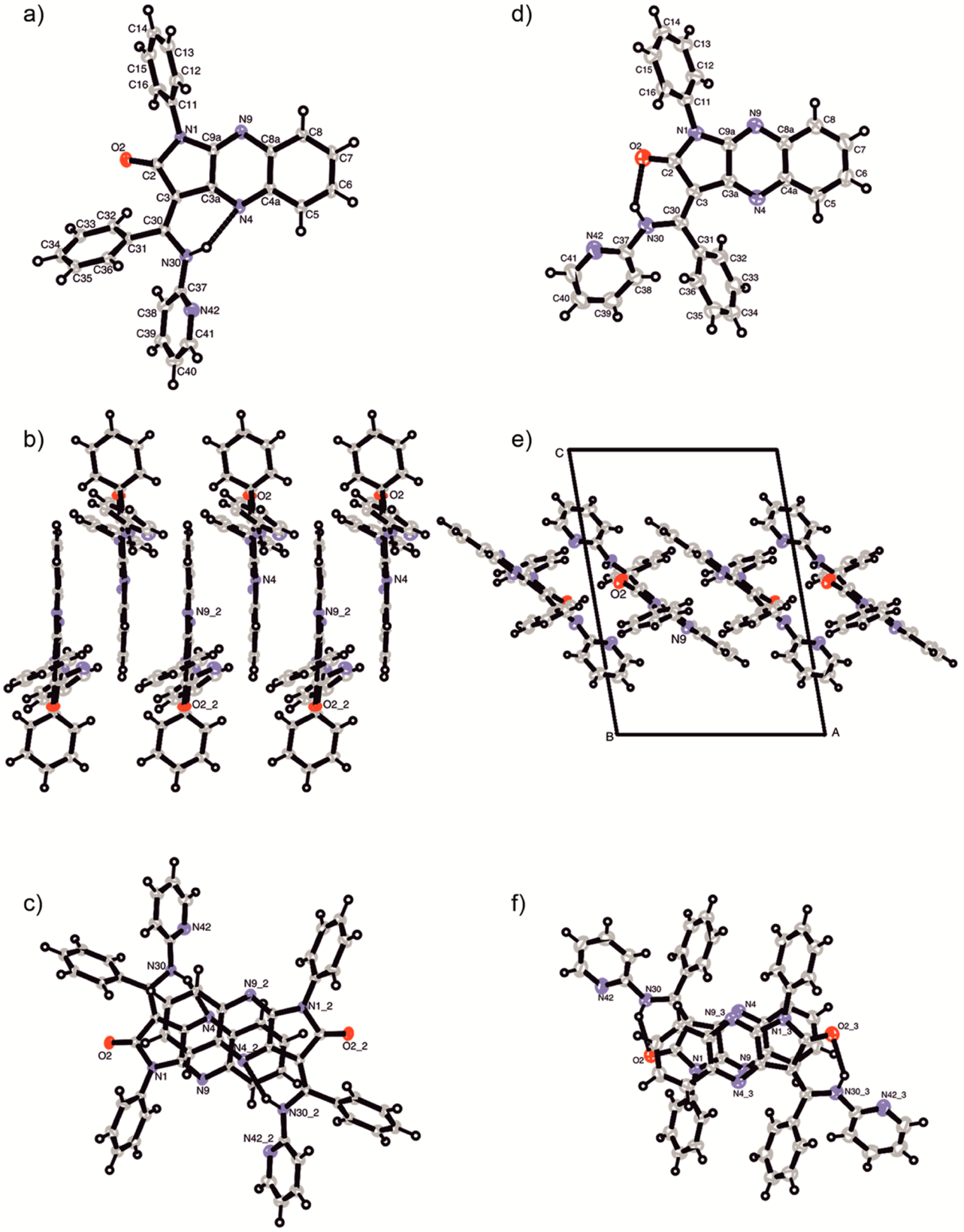

Figure 2. (a) ORTEP[26] view of molecule (*E*)-**2** with the atom numbering scheme. (b) (*E*)-**2**: packing of the molecules viewed along [010]. (c) Relationship of two neighboring fluorophores with an interplanar distance of 3.287 Å. (d) ORTEP view of molecule (*Z*)-**2**. (e) (*Z*)-**2**: packing of the molecules viewed along [010]. (f) Centrosymmetric dimers of (*Z*)-**2** in the crystal structure of (*Z*)-**2**. The non-hydrogen atoms are represented as displacement ellipsoids at 50% probability levels.

DOI: 10.1021/acs.inorgchem.5b01533
Inorg. Chem. 2015, 54, 8423−8435

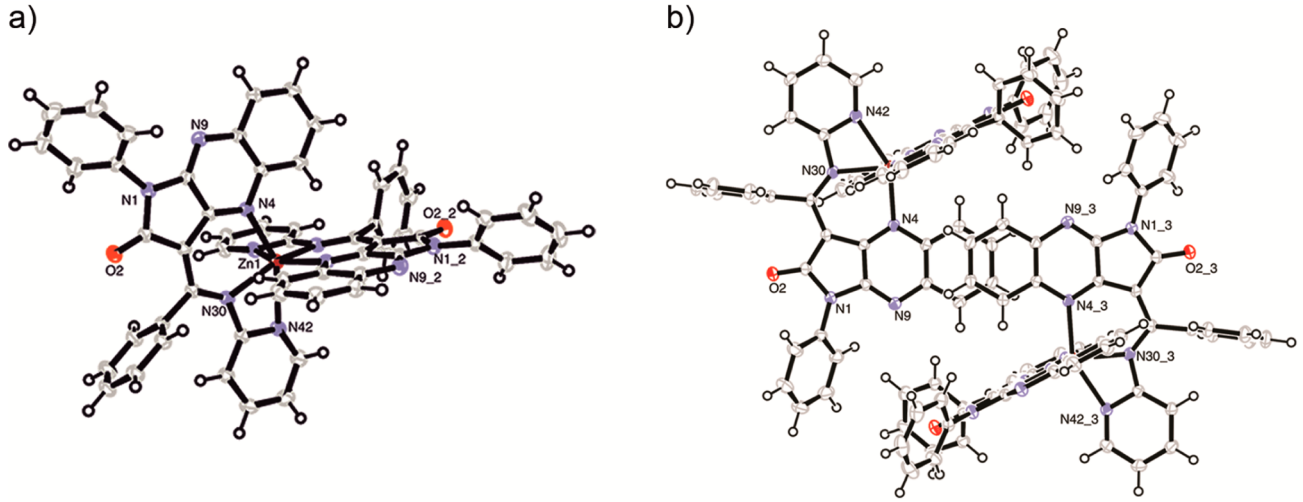

Figure 3. (a) ORTEP view of molecule $[(E)\text{-}\mathbf{2}]_2$Zn with the atom numbering scheme. (b) Relationship of two neighboring fluorophores with an interplanar distance of 3.502 Å.

Table 1. Free Enthalpy $\Delta G°$ and Barriers to Rotation $\Delta G^{‡}$ Estimated for (*E*/*Z*)-2 and (*E*/*Z*)-3

	$\Delta G°$(DMSO-d_6) [kcal mol^{-1}]				$\Delta G^{‡}$(DMSO-d_6) [kcal mol^{-1}]		
					TopSpin DNMR line-shape analyses, Eyring equation		
	DMSO-d_6	CD_3CN	CD_3OD	*TopSpin*	*E*→*Z*	*Z*→*E*	$\Delta G^{‡} = f(T_c)$, Eyring equation
experimental (^{1}H NMR)	0.718 (**2**)	0.778 (**2**)	1.399 (**2**)	0.8 (**2**, DMSO-d_6)	19.3 ± 0.1 (**2**)[a]	18.5 ± 0.2 (**2**)[a]	17.62 (**2**)
	0.831 (**3**)	0.839 (**3**)	1.269 (**3**)	1.2 (**3**, $CDCl_3$)	16.9 ± 0.3 (**3**)[b]	15.7 ± 0.2 (**3**)[b]	

[a]DMSO-d_6. [b]$CDCl_3$.

constant ^3J = 4.9 Hz are assigned to proton (*E*/*Z*)-H_a of the pyridyl groups (Figure 2). Deshielding of (*E*/*Z*)-H6′ for all of the diastereoisomers also indicates the participation of the pyridyl nitrogen atom in the formation of intramolecular hydrogen bonds with four- and six-membered rings in solution. The more upfield-shifted (*E*)-H_a proton is observed for ligand **3**. The most downfield-shifted signals are observed for acidic (*E*/*Z*)-NH protons in ligand **2** because of an additional resonance effect at amidine-resembling moieties.

Complex $[(E)\text{-}\mathbf{2}]_2$Zn was easily obtained during heating of **2** with $Zn(OAc)_2$ or $Zn(acac)_2$ in MeOH for 5 min.

X-ray Crystal Structure Analysis of (*E*)-2, (*Z*)-2, and $[(E)\text{-}\mathbf{2}]_2$Zn. Single crystals of both the *E* and *Z* diastereoisomers of **2** and the $[(E)\text{-}\mathbf{2}]_2$Zn complex were obtained (Supporting Information), and their crystal structures were determined experimentally. Form (*E*)-**2** was isolated from MeOH or DMSO-d_6 and (*Z*)-**2** from CH_3CN upon exposure to sunlight. X-ray crystal structure analysis of (*E*)-**2** and (*Z*)-**2** confirmed the configurations shown in Figure 2a,d. These configurations are stabilized by intramolecular hydrogen bonds between NH and N4 for the *E* isomer [N30−H30···N4, 2.05(2) and 2.839(3) Å, ∠DHA 143(3)°] and between NH and O of the imide carbonyl group for the *Z* form [N30−H30···O2, 1.98(1) and 2.715 Å, ∠DHA 137(1)°]. In addition, both of the *E*/*Z* forms in the crystalline state are related by $\pi-\pi$ noncovalent interactions between the pyrrolo[2,3-*b*]quinoxaline heterocyclic systems (Supporting Information and Figure 2b,c,e,f). The crystals of isomer *E* are assembled by strong $\pi-\pi$ interactions with a distance of 3.287 Å between the fused rings, which form a crystal framework through stacking arrangements along the *b* axis [010] following the space group $P2_1$. Diastereoisomer *Z* forms dimers containing the pair of enantiomers in a head-to-tail fashion and an interlayer distance of 3.667 Å within the space group $P2_1/c$. Dimers are formed by CH−π interactions between CH of the phenyl group at the N1 position and the pyridyl π donor (C16−H16···Cg6 and C15−H15···Cg6) with distances of 2.65 and 2.80 Å (Supporting Information), respectively.

The comparison of some bond lengths and valence, torsion, and dihedral angles for (*E*)-**2** and (*E*)-**3**[22] are given in Table 5 in Supporting Information. X-ray crystal structure analysis of (*E*)-**2** and (*E*)-**3** shows that both ligands form intramolecular hydrogen bonds between enamine NH and N4 with the planar six-membered rings and with the shortening of the C30−N30 bonds to a length corresponding to the double bond. Introduction of the flexible ethylene spacer between the fluorophore and pyridyl group could enable the formation of additional hydrogen bonds between enamine NH and pyridyl nitrogen with the lower-strain conformation in the case of ligand **3**.

X-ray analysis of $[(E)\text{-}\mathbf{2}]_2$Zn single crystals shows a six-coordinated structure of the zinc complex in which the nitrogen atoms (N4, N30, and N42) of both ligands coordinate to zinc, forming six- and four-membered bis-chelate rings (Figure 3). The structure is formed because of $\pi-\pi$ and lone pair−π noncovalent interactions between the fused benzene ring in pyrroloquinoxaline, with a distance of 3.859 Å between the appropriate benzene ring gravity centers (Cg−Cg; Figure 3b) and the carbonyl oxygen O2 and the phenyl ring at C30 within a distance of 3.363 Å. A methanol molecule included during crystallization stabilizes the crystal structure through additional hydrogen-bond formation between the carbonyl oxygen O2 and the methanol hydroxyl group (Supporting Information).

DOI: 10.1021/acs.inorgchem.5b01533
Inorg. Chem. 2015, 54, 8423−8435

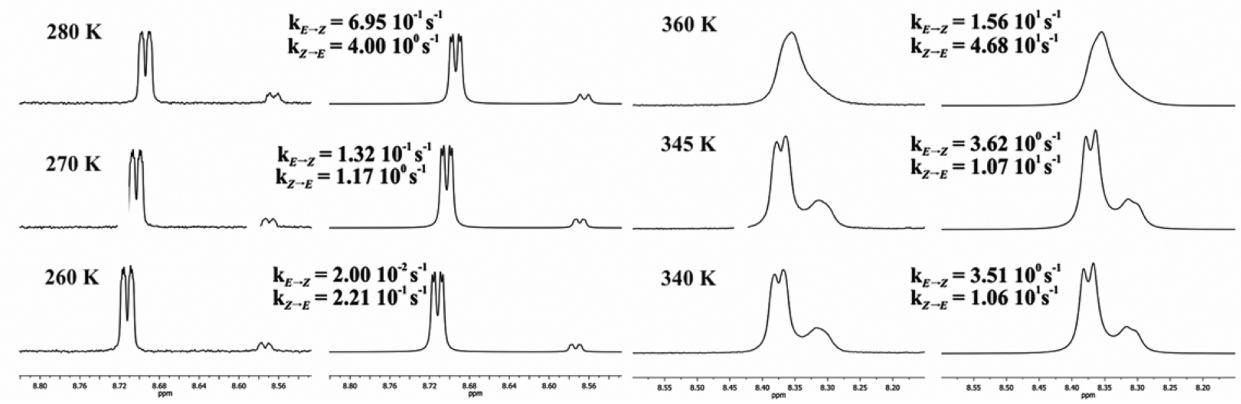

Figure 4. Temperature-dependent 300 MHz ^{1}H NMR spectra of the experimental and calculated H_a signals for (*E*/*Z*)-**2** (right) and (*E*/*Z*)-**3** (left). Experimental spectra and line-shape simulation were obtained with the rate constants indicated in the calculated spectra for temperatures of 340, 345, and 360 K for **2** (DMSO-d_6) and 260, 270, and 280 K for **3** ($CDCl_3$).

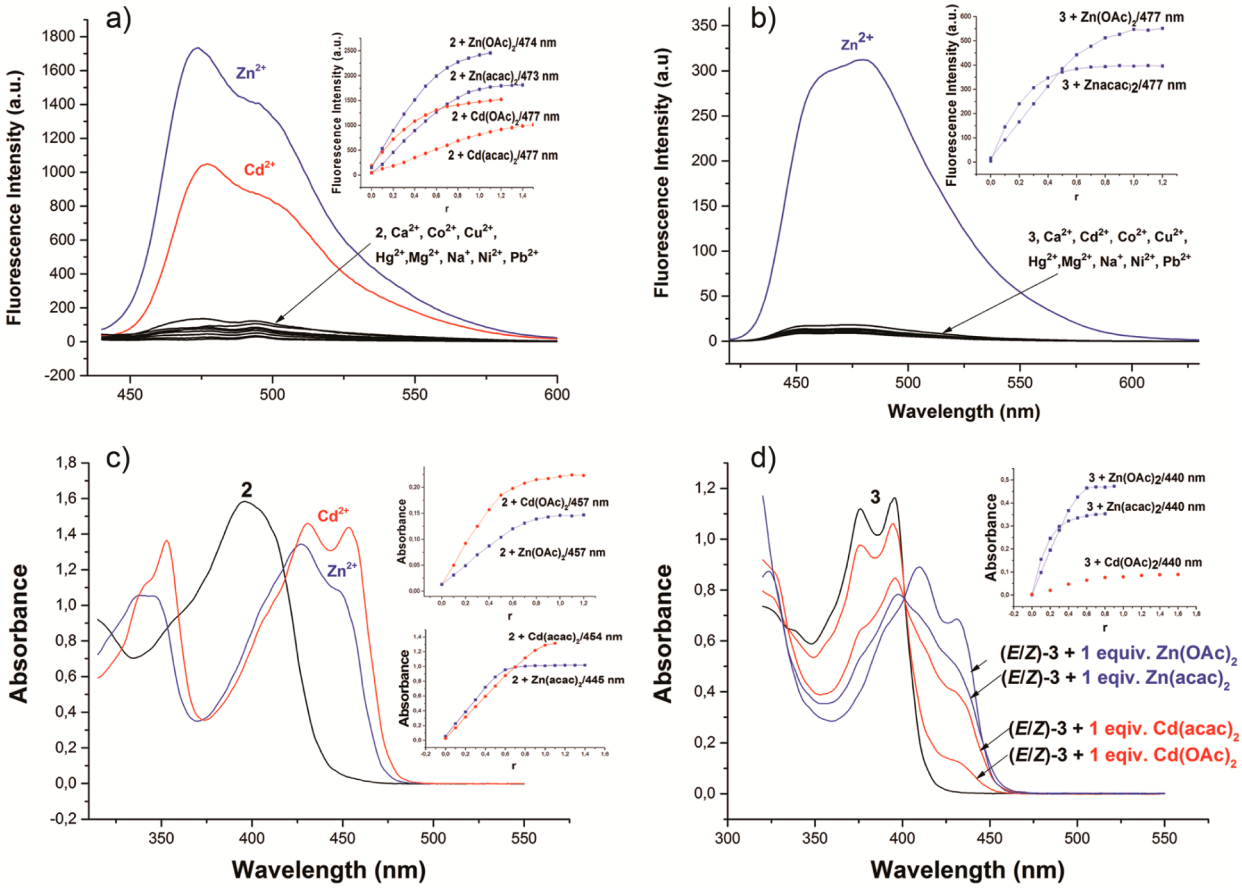

Figure 5. (a) Fluorescence spectra of **2** (10 μM) in CH_3CN with 1 equiv each of Zn^{2+}, Cd^{2+}, Hg^{2+}, Na^{+}, Mg^{2+}, Pb^{2+}, Ni^{2+}, Co^{2+}, Ca^{2+}, and Cu^{2+} (λ_{ex} = 430 nm). Inset: Increase in the fluorescence intensity at λ_{em} = 473 nm and λ_{em} = 477 nm as a function of 1 equiv of $Zn(OAc)_2$, $Zn(acac)_2$ and $Cd(OAc)_2$, $Cd(acac)_2$, respectively. (b) Fluorescence spectra of **3** (10 μM) in CH_3CN with 1 equiv each of Zn^{2+}, Cd^{2+}, Hg^{2+}, Na^{+}, Mg^{2+}, Pb^{2+}, Ni^{2+}, Co^{2+}, Ca^{2+}, and Cu^{2+} (λ_{ex} = 410 nm). Inset: Increase in the fluorescence intensity at λ_{em} = 477 nm as a function of 1 equiv of $Zn(OAc)_2$ and $Zn(acac)_2$. (c) Absorption spectra of **2** (50 μM) in CH_3CN with 1 equiv each of $Zn(OAc)_2$ and $Cd(OAc)_2$. Inset: Increase in the absorbance of **2** (10 μM) in CH_3CN at λ = 457 nm for $Zn(OAc)_2$ and $Cd(OAc)_2$, λ = 445 nm for $Zn(acac)_2$, and λ = 454 nm for $Cd(acac)_2$ as a function of 1 equiv of the salts. (d) Absorption spectra of **3** (50 μM) in CH_3CN with 1 equiv of Zn^{2+}, Cd^{2+}, Hg^{2+}, Na^{+}, Mg^{2+}, Pb^{2+}, Ni^{2+}, Co^{2+}, Ca^{2+}, and Cu^{2+}. Inset: Increase in the absorbance of **3** (10 μM) in CH_3CN at λ = 440 nm as a function of 1 equiv of $Zn(OAc)_2$, $Zn(acac)_2$, and $Cd(acac)_2$, respectively.

Barrier to Rotation about the Enamine Double Bond. Both ligands have a push−pull architecture with an electron-donating enamino group and an electron-accepting carbonylamide moiety. The difference ΔG° between free enthalpies of the *Z* and *E* forms for **2** (Table 1) and **3** was obtained using equation $\Delta G^\circ = -RT \ln K$ (R = universal gas constant, T = temperature, and K = equilibrium constant).[30] The relative concentrations of (*Z*)-**2** and (*E*)-**2** were determined by integration of the corresponding signals from the ^{1}H NMR data (DMSO-d_6, CD_3CN, and MeOD at 300 K). With

DOI: 10.1021/acs.inorgchem.5b01533
Inorg. Chem. 2015, 54, 8423−8435

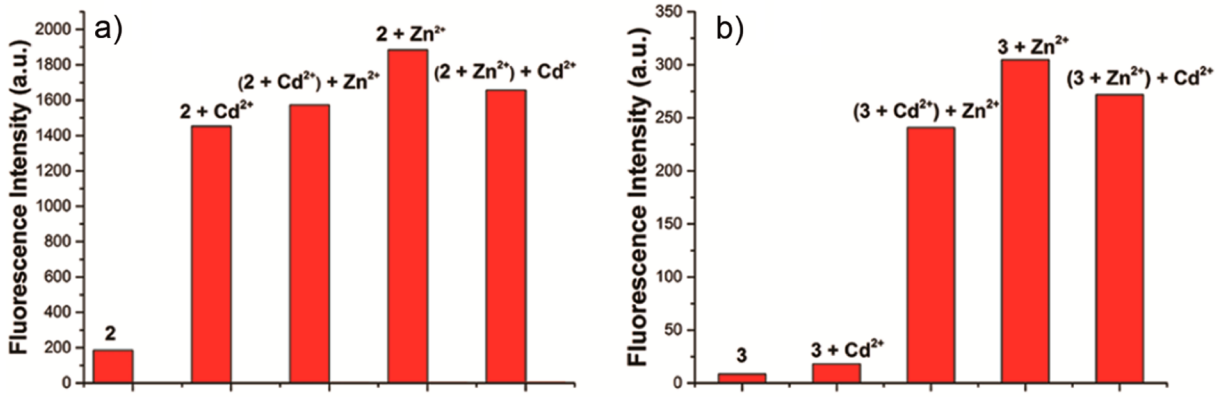

Figure 6. Metal-ion selectivity and competition profiles of (a) **2** (10 μM) in the presence of 1 equiv of $Zn(acac)_2$ or/and $Cd(acac)_2$ in CH_3CN at 430/476 nm. (b) **3** (10 μM) in the presence of 1 equiv of $Zn(acac)_2$ or/and $Cd(acac)_2$ in CH_3CN at 415/470 nm.

increasing solvent polarity,[31,32] the value of $\Delta G°$ increases. The energy differences between the isolated molecules of rotamers *E* and *Z* were calculated (Supporting Information) using two solvation models, a polarizable continuum model and a density-based solvation model, and the B3LYP functional and two basis sets, 6-31G* and 6-311G**, with *Gaussian09*.[33] The *E*/*Z* equilibrium for **2** was investigated by ^{1}H NMR at 310, 340, 345, 350, and 360 K (Figure 4 and the Supporting Information). The barrier to rotation about the enamine double bond that corresponds to the free enthalpy of activation $\Delta G^‡$ [cal mol^{-1}] was calculated from the Eyring equation (Table 1 and the Supporting Information).[30]

To compare the energetic barrier for the interconversion process, line-shape simulation was also performed using the dynamic ^{1}H NMR (DNMR) program of *TopSpin*[34] to calculate the rate constants and estimate the free enthalpy of activation ($\Delta G^‡$) (Figure 4 and Table 1).[35,36] Our calculation shows that the introduction of a 2-pyridyl group to the enamine nitrogen atom in **2** diminishes $\Delta G°$ between the free enthalpies of the *Z* and *E* forms and raises $\Delta G^‡$ in the case of the ethylene group in **3**. This difference is connected with expansion of the conjugation within the push−pull system.

UV−Vis and Fluorescence Spectra. The selective dual-emission responses are observed exclusively for **3** with zinc ion and for **2** with both zinc and cadmium ions in acetonitrile (Figure 5a,b). The fluorescence spectra in acetonitrile were recorded by excitation at a wavelength based on the 2D absorption−emission spectra of **2** and **3** with various metal ions such as Zn^{2+}, Cd^{2+}, Hg^{2+}, Na^+, Mg^{2+}, Pb^{2+}, Ni^{2+}, Co^{2+}, Ca^{2+}, and Cu^{2+}. The absorption spectra of ligands **2** and **3** showed two maxima at 395 and 415 nm for **2** and 376 and 396 nm for **3** in acetonitrile, which are attributed to the $\pi-\pi^*$ transitions (Figure 5c,d). To study the influence of the divalent zinc and cadmium ions on the UV−vis spectra of **2** and **3** in acetonitrile, we performed experiments between the ligands and 1 equiv of metal acetylacetonate and acetate salts, respectively. The zinc ions affect the absorption spectral profiles of **2** and **3**, showing a red-shifted band with the appearance of a new absorption maximum. The addition of cadmium acetate or acetylacetonate to **2** reveals a bathochromic shift of the absorption spectra from 395 and 415 nm to 429 and 453 nm, respectively. Ligand **3** shows weak interaction with the cadmium ion with a decrease in the intensity of the absorption maxima at 395 and 415 nm and the appearance of the new one at 430 nm (Figure 5d and Supporting Information).

The absorption spectroscopic titration of the ligands with zinc and cadmium acetate showed isosbestic points for **2** at 419 nm with $Zn(OAc)_2$, at 418 nm with $Zn(acac)_2$, and at 419 nm with $Cd(OAc)_2$ and $Cd(acac)_2$ and for **3** with $Zn(OAc)_2$, $Zn(acac)_2$, $Cd(OAc)_2$, and $Cd(acac)_2$ at 402 nm[22] (Supporting Information). The occurrence of isosbestic points indicates the formation of complexes without the involvement of intermediate products.

To determine the binding stoichiometry (Job's plot) of **2** with $Zn(OAc)_2$ and $Cd(OAc)_2$, the absorption of **2** was plotted as a function of the molar fraction of **2** under a constant total concentration of both **2** and metal ions. For both measurements, we observed the maxima at 0.66 that correspond to the formation of L_2M complexes with a 2:1 stoichiometry in solution.

The association constants (K_a) of **2** with zinc and cadmium ions were calculated by analyzing the titrations of acetate salts with (*E*/*Z*)-**2** in acetonitrile using UV−vis to monitor changes in the absorbance (Supporting Information). The data were analyzed using a nonlinear least-squares fit algorithm (*ReactLab Equilibria*[29]) for models M + L = ML, ML + L = ML2. The following overall stability constants were obtained: log β_{12} = 12.45 ± 0.127 with log K_1 = 6.76 ± 0.099 for Zn^{2+} and log β_{12} = 11.32 ± 0.057 with log K_1 = 6.61 ± 0.037 for Cd^{2+}.

Our subsequent investigations decisively showed that the ICT fluorescence enhancement of ligand **3** is connected via planarization of the fluorophore with the restriction of rotation around the exocyclic double bond at the 3 position of the pyrroloquinoxaline system.[22] Complex formation with deprotonation of the NH enamine group should inhibit *E*/*Z* isomerization. The planarization is possible by coordination of the metal ion through enamine and N5 atoms, which was indicated by X-ray analysis of [(*E*)-**2**]$_2$Zn and (*E*)-**3**-ZnOAc. We observed a series of equilibria in solution, such as *Z*/*E* isomerization, coordination with binding mode 1:1 by the *E* form of the ligand, and further complex formation with binding mode 2:1. UV−vis titration data, selectivity, and competition experiments (Figures 5 and 6) indicated that [*N*,*N*,*N*]-tridentate ligands **2** and **3** coordinate with zinc and cadmium ions in acetonitrile. The formation of complexes with zinc ions and ligands **2** and **3** proceed with planarization of the fluorophore. The appearance of a slightly intense bands at 430 nm in the UV−vis titration data for **3** and $Cd(OAc)_2$ or $Cd(acac)_2$ may be attributed to the formation of unstable complexes, constituted by enamine and pyridyl nitrogen donors. The devoid of the planarity fluorophore in complex

DOI: 10.1021/acs.inorgchem.5b01533
Inorg. Chem. 2015, 54, 8423−8435

Scheme 2. Proposed Binding Modes of 2 with $Zn(acac)_2$ and $Cd(OAc)_2$ and ^1H NMR Data for $[(E)\text{-}2]_2Zn$, (*E*)-2-Znacac, and $[(E)\text{-}2]_2Cd$ in CD_3CN

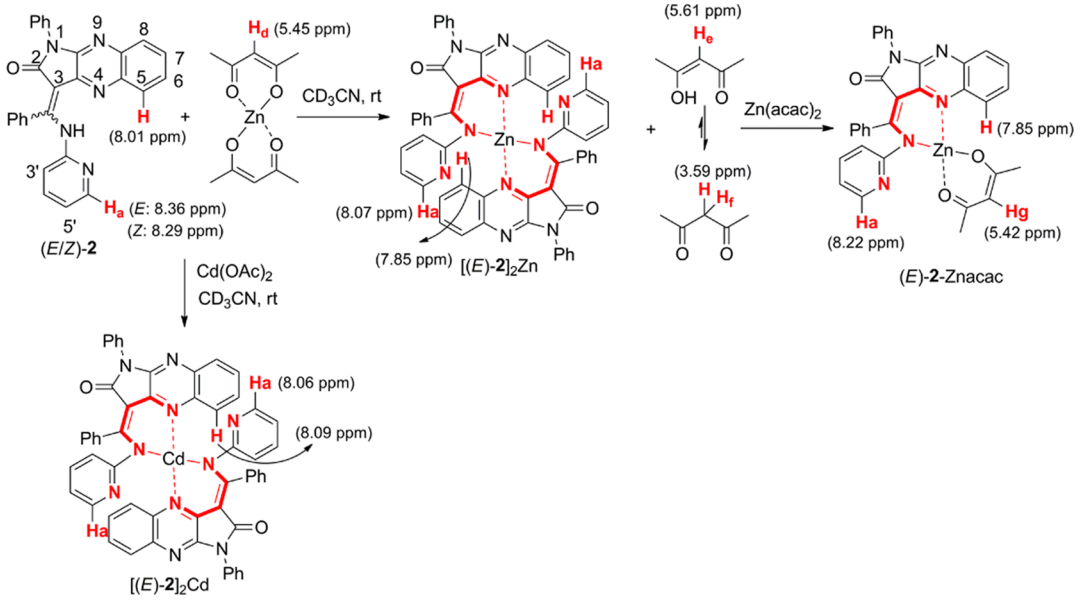

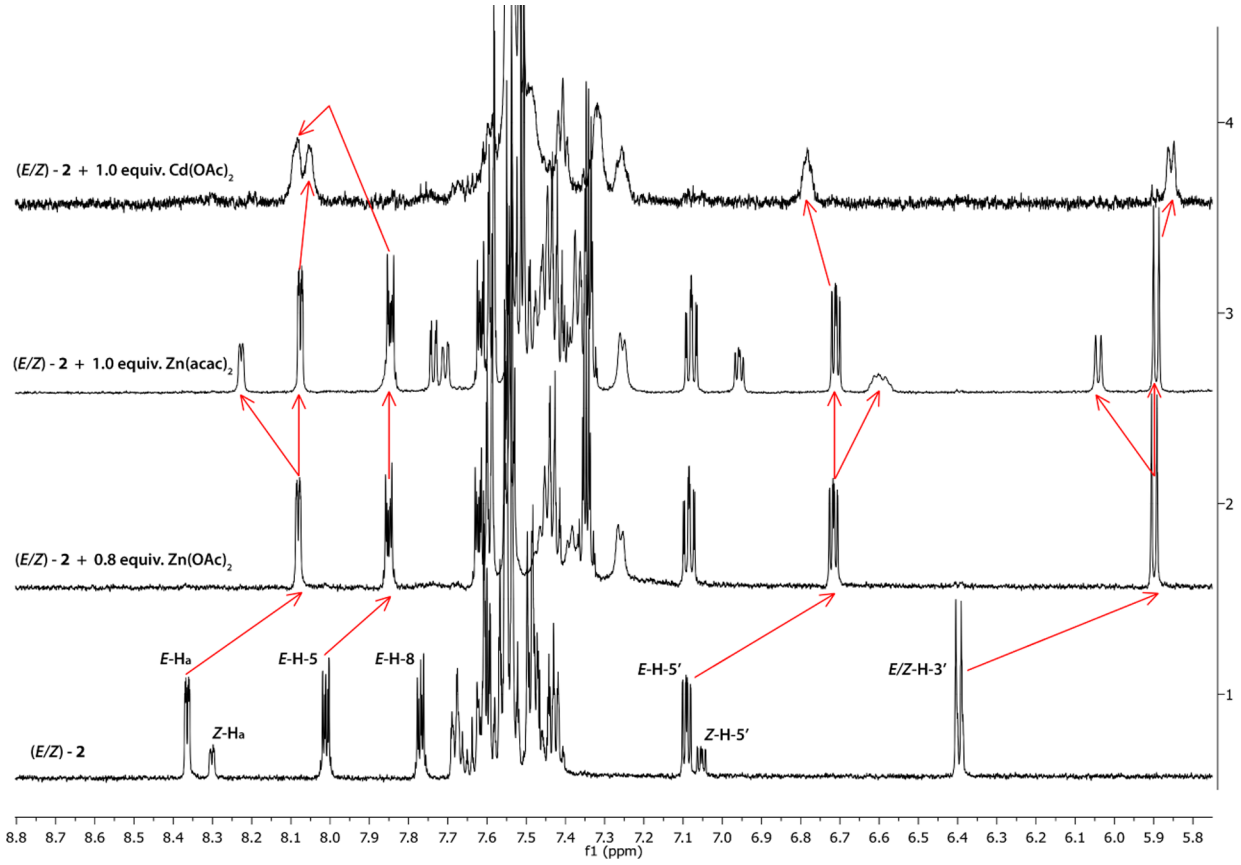

Figure 7. ^1H NMR spectra (600 MHz) of **2** (5 mM) in the presence of different concentrations of $Zn(OAc)_2$, $Zn(acac)_2$, and $Cd(OAc)_2$ in CD_3CN.

3-Cd could explain the very low fluorescent response of **3** to Cd^{2+} (Figures 5b and 6b).

^1H NMR Titration Data. The ^1H NMR titration of **2** with $Zn(OAc)_2$ and $Cd(OAc)_2$ in CD_3CN determined the formation of complexes $[(E)\text{-}2]_2M$ following the deprotonation of enamine (Scheme 2, Figure 7, and the Supporting Information). The X-ray crystal structure analysis of $[(E)\text{-}2]_2Zn$ confirmed the formation of a six-membered complex with binding mode 2:1 with two six-membered and two four-membered chelate rings. This complex is also formed during the ^1H NMR titration of **2** with zinc acetylacetonate in CD_3CN. However, the gradual addition of $Zn(acac)_2$ from 0.2 to 1.5 equiv showed reorganization of $[(E)\text{-}2]_2Zn$ to (*E*)-**2**-Znacac with a ligand-to-Zn^{2+} binding mode of 1:1. The reorganization

DOI: 10.1021/acs.inorgchem.5b01533
Inorg. Chem. 2015, 54, 8423−8435

Table 2. ^{1}H NMR Data for Diagnostic Protons

	(*E*)-H_a	(*Z*)-H_a	(*E*)-H_b	(*Z*)-H_b	(*E*)-H_c	(*Z*)-H_c	H_g
2	8.36	8.29					
3	8.62	8.50	3.12 (t)	3.05 (t)	3.76 (q)	3.70 (q)	
[(*E*)-**2**]$_2$Zn	8.08						
[(*E*)-**2**]$_2$Zn[a]	8.04						
(*E*)-**2**-Znacac	8.23						5.42
[(*E*)-**3**]$_2$Zn	8.16		2.81−2.77 (m) 2.89−2.84 (m)		3.31 (t)		
(*E*)-**3**-Znacac	8.56		3.15		3.56		5.44
(*E*)-**3**-ZnOAc	8.75		3.33		3.63		

[a]DMSO-d_6.

Scheme 3. Proposed Binding Modes of 3 with Zn(acac)$_2$

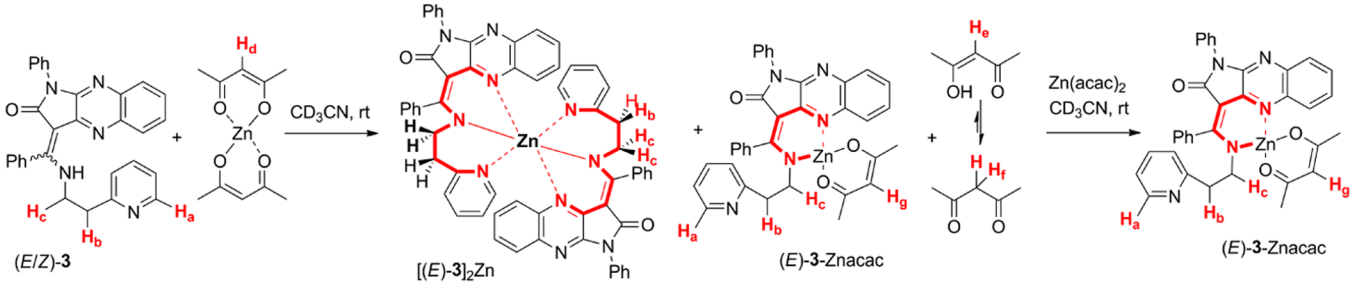

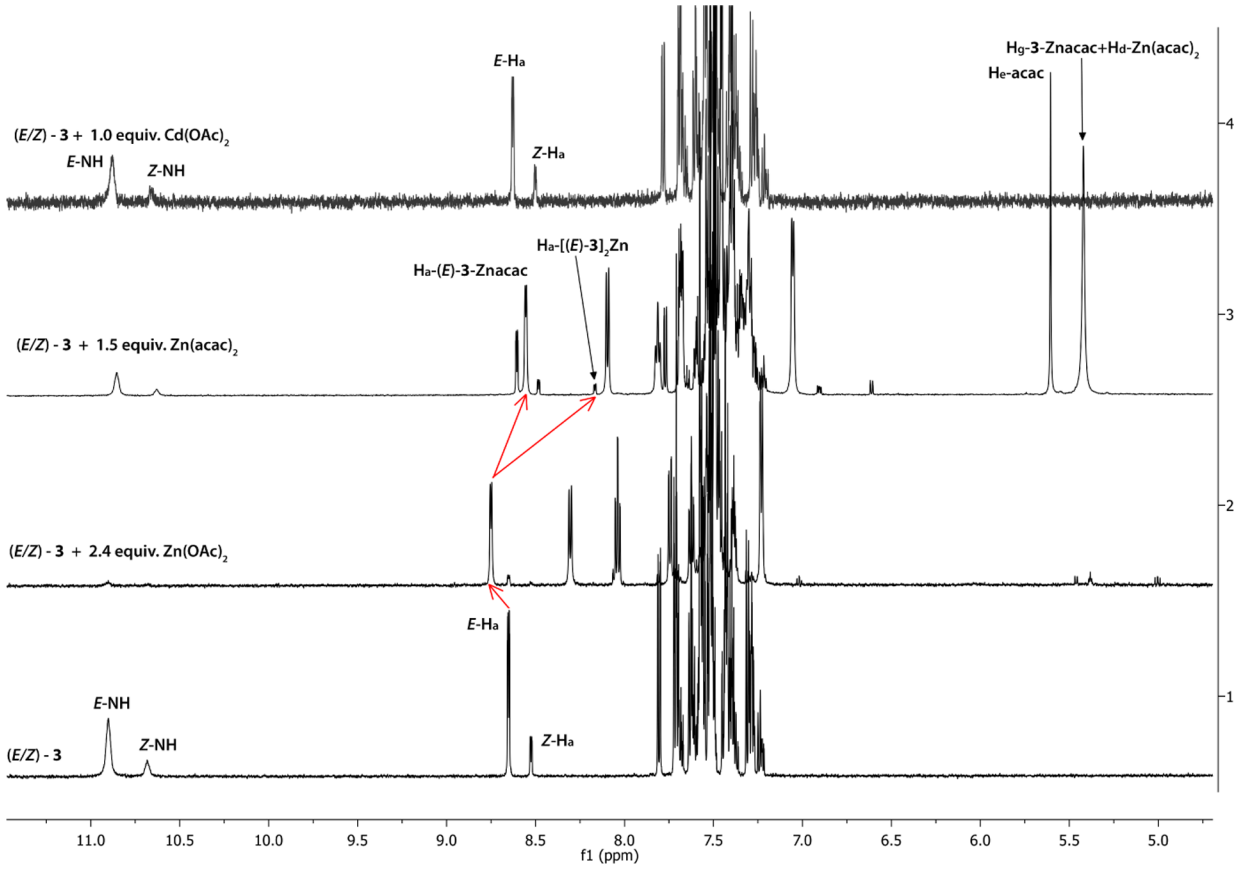

Figure 8. ^{1}H NMR spectra (600 MHz) of **3** (5 mM) in the presence of different concentrations of Zn(OAc)$_2$, Zn(acac)$_2$, and Cd(OAc)$_2$ in CD$_3$CN.

was assessed by the appearance of an additional set of signals, with a singlet at 5.42 ppm attributed to H_g of (*E*)-**2**-Znacac and a doublet at 8.22 ppm with the diagnostic coupling constant ^3J = 4.5 Hz assigned to H_a. Both signals have the same population. One signal for two methyl groups of acac indicated that both oxygen atoms of acac coordinate to zinc. Application of zinc acetylacetonate, with proton H_d at 5.45 ppm, as a counter salt in ^{1}H NMR titration enables tracking of the complex formation by tracing the characteristic signals of the two tautomeric forms of acetylacetone, such as H_e at 5.61 ppm, OH at 15.58 ppm,

DOI: 10.1021/acs.inorgchem.5b01533
Inorg. Chem. 2015, 54, 8423−8435

Table 3. Properties of the BCPs for the Closed-Shell Zinc−Oxygen and Zinc−Nitrogen Interactions: Charge Density (Atomic Units, au) = $\rho(r)$, Laplacian (au) = $\nabla^2\rho(r)$, and Eigenvalues of Hessian (au) = λ_1, λ_2, and λ_3, Internuclear Separations (Å) = R_{ij}, Distance between BCPs and Atoms 1 and 2, Respectively (Å) = d_1 and d_2, and Local Kinetic and Local Potential Energy Densities, Respectively (au) = $V(r_{CP})$ and $G(r_{CP})$

	$\rho(r)$	$\nabla^2\rho(r)$	R_{ij}	d_1	d_2	$G(r_{CP})$	$V(r_{CP})$	$E(r_{CP})$	$\lvert V(r_{CP})\rvert/G(r_{CP})$	$E(r_{CP})/\rho(r)$
					(*E*)-**3**-ZnOAc					
Zn1−O3	0.09	0.43	1.95	0.943	1.011	0.13	−0.14	−0.02	1.13	−0.18
Zn1−N4	0.09	0.35	1.99	0.952	1.039	0.11	−0.14	−0.02	1.22	−0.27
Zn1−N30	0.09	0.32	2.02	0.964	1.058	0.10	−0.13	−0.02	1.22	−0.27
Zn1−N44a	0.08	0.29	2.06	0.981	1.079	0.09	−0.11	−0.02	1.21	−0.25
$[(E)$-**2**$]_2$Zn										
Zn1−N30	0.07	0.23	2.116	1.006	1.111	0.08	−0.09	−0.02	1.23	−0.25
Zn1−N4	0.06	0.21	2.149	1.020	1.129	0.07	−0.08	−0.02	1.22	−0.24
Zn1−N42	0.05	0.15	2.261	1.081	1.181	0.05	−0.06	−0.01	1.21	−0.21

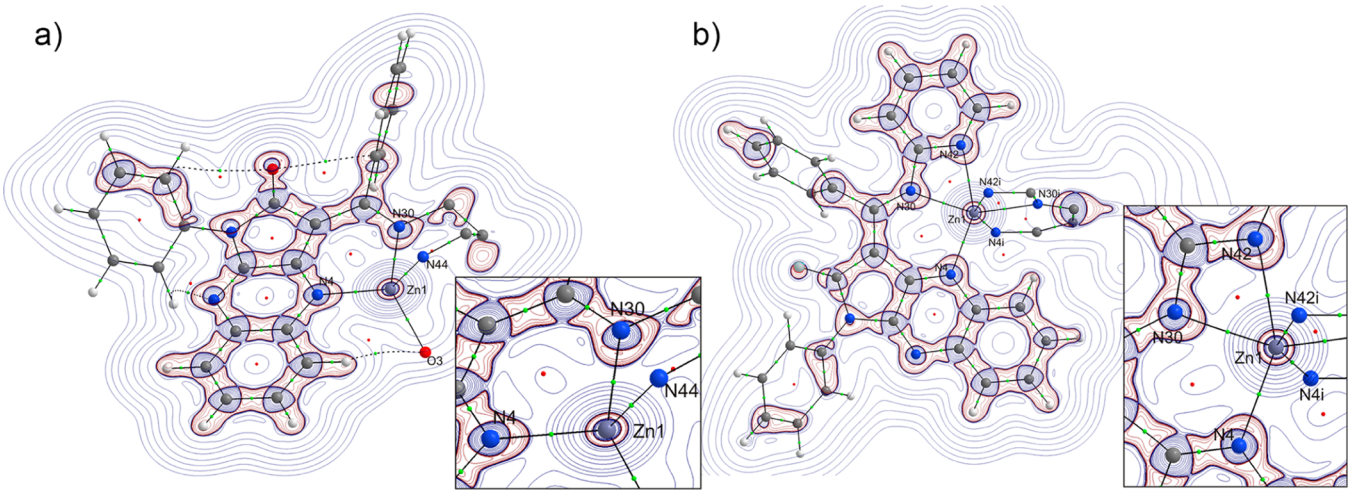

Figure 9. Laplacian map in the plane of (a) N4−Zn1−N30 for (*E*)-**3**-ZnOAc and (b) N4−Zn1−N30 for $[(E)$-**2**$]_2$Zn with marked (3, −1) critical points and (3, +1) critical points. The enhanced figures show the distribution of the lone pairs around nitrogen atoms connected to the zinc central atom in both complexes. Contours are at logarithmic intervals in $-\nabla^2\rho(r)$ (e Å^{-5}).

and H_f at 3.59 ppm, following the reactions in Scheme 2 (Figure 7, Table 2, and the Supporting Information). The binding stoichiometry for complexes L_2Zn or LZnacac could be determined through the lack or appearance of a new singlet in the alkene region, respectively.

^{1}H NMR titration of **2** with $Cd(OAc)_2$ in CD_3CN showed only one set of signals ascribed to $[(E)$-**2**$]_2$Cd, which was formed from deprotonation of the ligand. The NMR data showed that signal H5 at 8.06 ppm of the cadmium complex was downfield-shifted in contrast to H5 at 7.85 ppm of $[(E)$-**2**$]_2$Zn and (*E*)-**2**-Znacac. This may suggest that cadmium, with the longer ionic radius, forms a complex with a geometry that is distorted in relation to $[(E)$-**2**$]_2$Zn. ^{13}C NMR data of (*E*/*Z*)-**2** with 1 equiv of $Cd(OAc)_2$ in DMSO-d_6 precluded the coordination of Cd^{2+} with the carbonyl oxygen, showing a chemical shift for carbon of the carbonyl imide group similar to that for the ligand and the $[(E)$-**2**$]_2$Zn complex at 169.2, 168.91, and 169.84 ppm. We were not able to separate the complex from the reaction mixture of (*E*/*Z*)-**2** with acetate or acetylacetonate cadmium salts in MeOH. The excess of cadmium acetate added to the reaction mixture induces crystallization of one (*E*)-**2** diastereoisomer exclusively.

Complex (*E*)-**3**-ZnOAc with a binding mode of 1:1 was published previously.[22] Replacement of zinc acetate by zinc acetylacetonate changed the mechanism of complex formation. ^{1}H NMR titration indicates the formation of two complexes, $[(E)$-**3**$]_2$Zn and (*E*)-**3**-Znacac, upon the addition of 0.2 equiv of $Zn(acac)_2$ to **3** in CD_3CN. Further, the addition of zinc ions showed the following reorganization: $[(E)$-**3**$]_2$Zn to (*E*)-**3**-Znacac (Scheme 3, Figure 8, and Supporting Information). The addition of cadmium acetate to (*E*/*Z*)-**3** in CD_3CN does not induce deprotonation of enamine in (*E*/*Z*)-**3**. We observed two sets of signals from the unbound *E* and *Z* diastereoisomers of **3**. The lack of complex formation could be explained by a lower acidity of the (*E*/*Z*)-NH proton in **3** in relation to (*E*/*Z*)-NH in **2** and also Cd^{2+} in relation to Zn^{2+}.

^{1}H NMR titrations of ligands **2** and **3** with zinc acetylacetonate in acetonitrile showed the formation of complexes with a binding mode of 2:1 and their further conversion to 1:1 upon the addition of metal salts. These reorganizations are not observed in the UV−vis titration spectra (Figure 5c,d).

Density Functional Theory (DFT) Calculations. Ab initio calculations were performed for the isolated molecules of (*E*)-**3**-ZnOAc and $[(E)$-**2**$]_2$Zn at the DFT/B3LYP level of theory using the 6-31++G(d,p) basis set. The molecular geometry for the "wave-function" calculations[33] was taken from the crystal structure and modified assuming the C−H bond lengths from the neutron diffraction data.[37] The obtained wave function was used for the charge density calculations using the QTAIM approach implemented in the *AIMAll* software.[38] Analysis of the Laplacian of electron density and energetic

DOI: 10.1021/acs.inorgchem.5b01533
Inorg. Chem. 2015, 54, 8423−8435

criteria based on local potential and kinetic energy densities indicated the intermediate between closed-shell (ionic) and shared-shell (covalent) character of all Zn−N and Zn−O interactions: $E(r_{CP})/\rho(r) < 0$, $< 1|V(r_{CP})|/G(r_{CP}) < 2$, and $\nabla^2\rho(r) > 0$ (Table 3). Higher values of the Laplacian for zinc−nitrogen bonds in (*E*)-**3**-ZnOAc than for $[(E)\text{-}\mathbf{2}]_2$Zn indicate their more ionic character. This can be correlated with shortening of the zinc−nitrogen bonds upon moving from $[(E)\text{-}\mathbf{2}]_2$Zn to (*E*)-**3**-ZnOAc. The Zn1−N42 bond, which participates in the four-membered Zn1−N30−C37−N42 ring in $[(E)\text{-}\mathbf{2}]_2$Zn, can be considered the weakest among the zinc−nitrogen bonds. The values of the Laplacian at the bond critical point (BCP) and the distribution of lone pairs around nitrogen atoms (as seen up close in Figure 9a,b in the magnified coordination environment of the zinc central atom) indicate that six-membered rings based on zinc and nitrogen atoms are more stable than the four-membered ones. This can be considered as a result of sterical hindrance arising from the dense packing of two organic ligands around the zinc central ion. As expected the Zn1−O3 interaction in (*E*)-**3**-ZnOAc has more pronounced closed-shell (ionic) character compared to the zinc−nitrogen bonds, as seen by the more positive value of the Laplacian at BCP. The analysis based solely on the characterization of BCP around the zinc central atom suggests that the $[(E)\text{-}\mathbf{2}]_2$Zn complex should be more stable than the (*E*)-3-ZnOAc one.

Net atomic charges were calculated for all non-hydrogen atoms according to QTAIM and are summarized in Table 4.

Table 4. Net Atomic Charges for Zinc, Oxygen, and Nitrogen Atoms in (*E*)-3-ZnOAc and $[(E)\text{-}\mathbf{2}]_2$Zn

	q				
	Zn1	N4	O3	N30	N42/N44a
$[(E)\text{-}\mathbf{2}]_2$Zn	+1.266	−1.022		−1.085	−1.027
(*E*)-**3**-ZnOAc	+1.263	−1.079	−1.222	−1.058	−1.040

The Zn1 charge is similar in both complexes, and it is in agreement with the values obtained for other zinc organic complexes.[39−41] Dipole moments were calculated for the isolated complexes using the B3LYP functional and 6-311++G(2d,2p) basis sets. Different coordination modes differentiate the dipole moments for $[(E)\text{-}\mathbf{2}]_2$Zn (6.04 D) and (*E*)-**3**-ZnOAc (9.87 D).

Analysis of Coordination Spheres of $[(E)\text{-}\mathbf{2}]_2$Zn and (*E*)-3-ZnOAc. X-ray analysis of $[(E)\text{-}\mathbf{2}]_2$Zn and (*E*)-**3**-ZnOAc showed their different coordination cavities. [*N*,*N*,*N*]-Tridentate ligands, varying solely in the ethylene linker between the fluorophore and the ionophore pyridyl group, form six- and four-coordinated zinc central ions, respectively (Figure 10). The zinc atom is within 0.063(1) Å of the plane defined by the nitrogen donors N4, N30, and N42/44 in $[(E)\text{-}\mathbf{2}]_2$Zn and 2.333(2) Å in (*E*)-**3**-ZnOAc. Six-coordinated Zn^{2+} lengthens the zinc−nitrogen bonds because of the larger cavity size in relation to four-coordinated Zn^{2+} (Table 5 and Table 5 in the Supporting Information). The chelate effect and chelate ring size stabilize the formation of a structure with six- and four-membered bis-chelate rings in $[(E)\text{-}\mathbf{2}]_2$Zn. The greater coordination number weakens the strength of the metal−donor interaction and extends the length of the zinc−nitrogen bonds that diminish the overlap of zinc with the donor orbital. The average zinc−nitrogen bond length for bipyridyl sp^2-hybridized nitrogen atoms in octahedral complexes with five-membered chelate rings is 2.13 ± 0.05 Å.[14,16,19] A larger cavity size allows the coordination of a cadmium ion possessing a larger ionic radius (0.95 Å for six-coordinated metal ion) than zinc.

The determinant in selective zinc ion recognition by **3** is the formation of a distorted tetrahedral structure with a small coordination cavity. The flexible ethylene linker enables the formation with zinc of the additional six-membered chelate ring in a boat conformation with low strain. X-ray structure analysis of the (*E*)-**3**-ZnOAc single crystal indicates that the lengths of all zinc−nitrogen bonds are shorter than the lengths of the corresponding bonds in $[(E)\text{-}\mathbf{2}]_2$Zn. The small cavity size likely

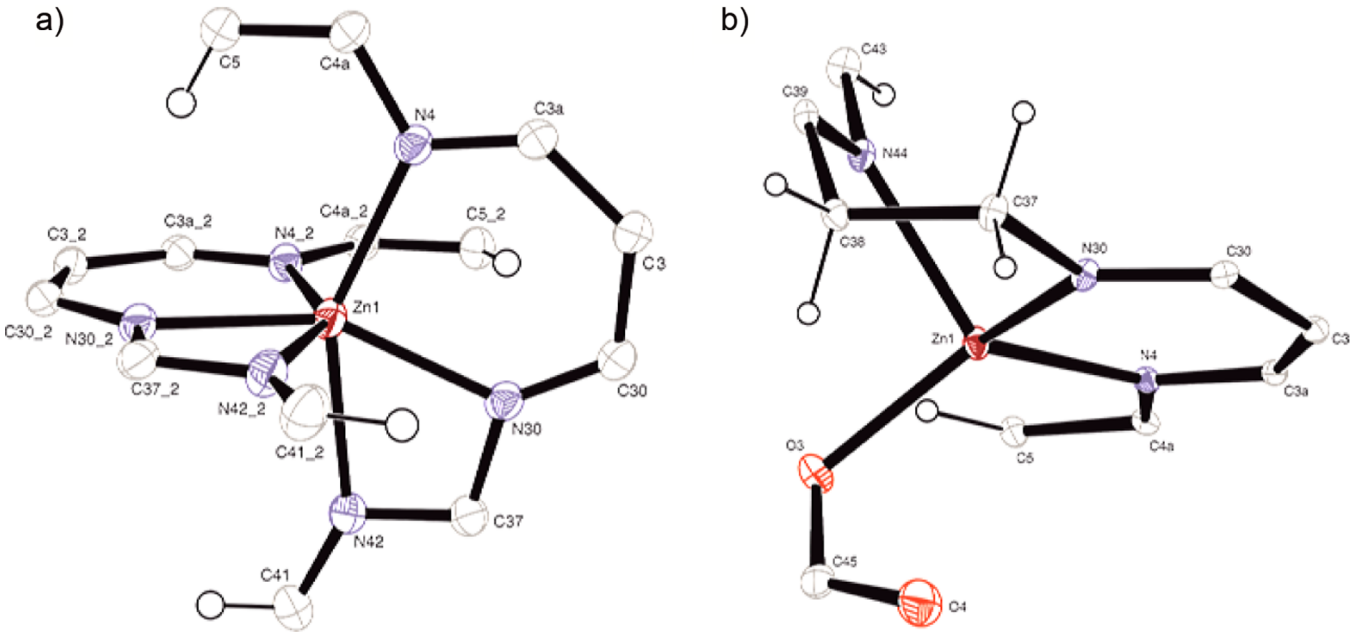

Figure 10. Coordination spheres of (a) $[(E)\text{-}\mathbf{2}]_2$Zn and (b) (*E*)-**3**-ZnOAc.

DOI: 10.1021/acs.inorgchem.5b01533
Inorg. Chem. 2015, 54, 8423−8435

Table 5. Geometry of Chelate Rings for $[(E)\text{-}2]_2$Zn and (*E*)-3-ZnOAc

	N4−M [Å]	N30−M [Å]	N42/N44a−M [Å]	valence angle N4−Zn−N30 [deg]	valence angle N30−Zn−N42/N44 [deg]	effective ionic radii for metal (coordination number) [Å]	log $K(CH_3CN)$
$[(E)$-**2**$]_2$Zn	2.1500	2.1169	2.2614	88.95	60.83	0.74 (6)	12.45
(*E*)-**3**-ZnOAc	1.9904	2.0225	2.0595	97.21	91.59	0.60 (4)	6.13

does not enable the coordination of a cadmium ion in the same manner as zinc. The ^{1}H NMR titration experiment of (*E*/*Z*)-**3** with $Cd(OAc)_2$ confirmed the presence of the *E*/*Z* equilibrium of **3** in CD_3CN and the lack of deprotonation of the enamine.

CONCLUSIONS

The coordination geometry of the complexes formed during binding is important for the design of a selective fluorescent sensor for zinc-ion recognition based on pyrrolo[2,3-*b*]-quinoxaline as the fluorophore. A distorted tetrahedral geometry of (*E*)-**3**-ZnOAc with a four-coordinated zinc ion appears to be the most preferred through the small coordination cavity size and short donor−zinc distance with a binding mode of 1:1. A determining factor for selective Zn^{2+} recognition is also the formation of six-membered chelate rings that provide an effective overlap of zinc with the donor orbital, which was confirmed by DFT calculations. The chelate effect in $[(E)\text{-}2]_2$Zn increases its affinity for metal ions and elongates the nitrogen metal bonds, extending the coordination cavity size.

ASSOCIATED CONTENT

Supporting Information

The Supporting Information is available free of charge on the ACS Publications website at DOI: 10.1021/acs.inorgchem.5b01533.

^{1}H NMR spectra of (*E*/*Z*)-**2** and $[(E)\text{-}2]_2$Zn, ^{13}C NMR spectra of (*E*/*Z*)-**2**; temperature-dependent 600 MHz ^{1}H NMR spectra of (*E*/*Z*)-**2** in DMSO-d_6, 2D fluorescence spectra of $[(E)\text{-}2]_2$Zn and (*E*/*Z*)-**2** with 1 equiv of $Cd(OAc)_2$, fluorescence spectra of (*E*/*Z*)-**2** upon the addition of $Zn(OAc)_2$ and $Cd(OAc)_2$, UV−vis absorption spectra of (*E*/*Z*)-**2** upon the addition of $Zn(OAc)_2$, UV−vis absorption spectra of (*E*/*Z*)-**2** upon the addition of $Cd(OAc)_2$ and Job's plot with $Cd(OAc)_2$, UV−vis absorption spectra of $Zn(OAc)_2$ upon the addition of (*E*/*Z*)-**2**, UV−vis absorption spectra of $Cd(OAc)_2$ upon the addition of (*E*/*Z*)-**2**, ^{1}H NMR spectra of (*E*/*Z*)-**2** upon titration with $Zn(OAc)_2$, $Zn(acac)_2$ and $Cd(OAc)_2$, and ^{1}H NMR spectra of (*E*/*Z*)-**3** upon titration with $Zn(acac)_2$, crystallographic data (PDF)

Crystallographic data (*E*)-**2** (CIF)

Crystallographic data (*Z*)-**2** (CIF)

Crystallographic data $[(E)\text{-}2]_2$Zn (CIF)

AUTHOR INFORMATION

Corresponding Author

*E-mail: ostrowsk@chemia.uj.edu.pl. Fax: +48-12-63-40-515.

Author Contributions

The manuscript was written through contributions of all authors. All authors have given approval of the final version of the manuscript.

Notes

The authors declare no competing financial interest.

†Crystal structure information. E-mail: stadnick@chemia.uj.edu.pl.

ACKNOWLEDGMENTS

The research was carried out with equipment purchased thanks to the financial support of the European Regional Development Fund in the framework of the Polish Innovation Economy Operational Program (Contract POIG.02.01.00-12-023/08). This research was supported, in part, by PL-Grid Infrastructure.

REFERENCES

(1) Vallee, B. L.; Falchuk, K. H. *Physiol. Rev.* **1993**, *73*, 79−118.

(2) Hyman, L. M.; Franz, K. J. *Coord. Chem. Rev.* **2012**, *256*, 2333−2356.

(3) Williams, R. J. P. *Zinc in human biology*; Mills, C. F., Ed.; Springer-Verlag: London, 1989; pp 15− 31.

(4) Chen, Y.; Bai, Y.; Han, Zh.; He, W.; Guo, Z. *Chem. Soc. Rev.* **2015**, *44*, 4475−4974. Maret, W. *Metallomics* **2015**, *7*, 202−211. Zhang, C.; Pu, Sh.; Sun, Zh.; Fan, C.; Liu, G. *J. Phys. Chem. B* **2015**, *119*, 4673−4682. Li, D.; Liu, L.; Li, W.-H. *ACS Chem. Biol.* **2015**, *10*, 1054−1063. Carter, K. P.; Young, A. M.; Palmer, A. E. *Chem. Rev.* **2014**, *114*, 4564−4601.

(5) Zhu, L.; Yuan, Zh.; Simmons, J. T.; Sreenath, K. *RSC Adv.* **2014**, *4*, 20398−20440.

(6) Choi, D. W.; Yokoyama, M.; Koh, J. *Neuroscience* **1988**, *24*, 67−79. Que, E. L.; Domaille, D. W.; Chang, Ch. J. *Chem. Rev.* **2008**, *108*, 1517−1549.

(7) Liu, Zh.; He, W.; Guo, Z. *Chem. Soc. Rev.* **2013**, *42*, 1568−1600.

(8) Martin, R. B. *Encyclopedia of Inorganic Chemistry*; King, R. B., Ed.;John Wiley & Sons Ltd.: New York, 1994; Vol. *4*, p 2195.

(9) Irving, H.; Williams, R. J. P.; Ferrett, D. J.; Williams, A. E. *J. Chem. Soc.* **1954**, 3494−3504.

(10) Hancock, R. D. *J. Chem. Educ.* **1992**, *69*, 615−621. Steed, J. W., Atwood, J. L. *Supromolecular Chemistry*; A John Wiley and Sons, Ltd., Publication: New York, 2009; pp 17−22 and 129−140.

(11) Mizukami, Sh.; Okada, S.; Kimura, S.; Kikuchi, K. *Inorg. Chem.* **2009**, *48*, 7630−7638.

(12) Goldsmith, Ch. R.; Lippard, S. J. *Inorg. Chem.* **2006**, *45*, 555−561.

(13) Xu, Zh.; Yoon, J.; Spring, D. R. *Chem. Soc. Rev.* **2010**, *39*, 1996−2006.

(14) Dai, Zh.; Canary, J. W. *New J. Chem.* **2007**, *31*, 1708−1718.

(15) Williams, N. J.; Gan, W.; Reibenspies, J. H.; Hancock, R. D. *Inorg. Chem.* **2009**, *48*, 1407−1415.

(16) Mikata, Y.; Wakamatsu, M.; Yano, Sh. *Dalton Transactions* **2005**, 545−550. Mikata, Y.; Yamanaka, A.; Yamashita, A.; Yano, Sh. *Inorg. Chem.* **2008**, *47*, 7295−7301.

(17) Mikata, Y.; Kawata, K.; Takeuchi, S.; Nakanishi, K.; Konno, H.; Itami, S.; Yasuda, K.; Tamotsu, S.; Burdette, Sh. C. *Dalton Transactions* **2014**, *43*, 10751−10759.

(18) Gan, W.; Jones, S. B.; Reibenspies, J. H.; Hancock, R. D. *Inorg. Chim. Acta* **2005**, *358*, 3958−3966.

(19) Andzyulene, B. K.; Vesene, T. B. *J. Appl. Spectrosc.* **1978**, *28*, 443−445.

(20) Nakamura, H.; Yoshida, T.; Todoko, M.; Ueno, K.; Takagi, M. *Bull. Chem. Soc. Jpn.* **1984**, *57*, 2839−2846.

(21) Hancock, R. D. *Chem. Soc. Rev.* **2013**, *42*, 1500−1524.

(22) Ostrowska, K.; Piegza, E.; Rąpała-Kozik, M.; Stadnicka, K. *Eur. J. Org. Chem.* **2012**, *19*, 3636−3646.

DOI: 10.1021/acs.inorgchem.5b01533
Inorg. Chem. 2015, 54, 8423−8435

(23) Ostrowska, K.; Kaźmierska, A.; Rąpała-Kozik, M.; Kalinowska-Tłuścik, J. *New J. Chem.* **2014**, *38*, 213−226.
(24) Ostrowska, K.; Dudek, Ł.; Grolik, J.; Gryl, M.; Stadnicka, K. *CrystEngComm* **2015**, *17*, 498−502.
(25) *CrysAlisPro*, version 1.171.33.66; Oxford Diffraction Ltd.: New Delhi, India.
(26) Altomare, A.; Cascarano, G.; Giacovazzo, C.; Guagliardi, A.; Burla, M. C.; Polidori, G.; Camalli, M. *J. Appl. Crystallogr.* **1994**, *27*, 435.
(27) Sheldrick, G. M. *Acta Crystallogr., Sect. A: Found. Crystallogr.* **2008**, *64*, 112−122.
(28) Farrugia, L. J. *J. Appl. Crystallogr.* **1997**, *30*, 565.
(29) Farrugia, L. J. *J. Appl. Crystallogr.* **1999**, *32*, 837−838.
(30) Thordarson, P. *Chem. Soc. Rev.* **2011**, *40*, 1305−1323.
(31) *ReactLab Equilibria*, version 1.1; Jplus Consulting Pty Ltd.: East Fremantle, Australia, 2013.
(32) Kessler, H. *Angew. Chem., Int. Ed. Engl.* **1970**, *9*, 219−235.
(33) Milart, P.; Stadnicka, K. *Liebigs Ann. /Recueil/* **1997**, *1997*, 2607−2611.
(34) Reichardt, Ch. *Pure Appl. Chem.* **2004**, *76*, 1903−1919.
(35) Frisch. M. J.; et al. *Gaussian 09*, revision A.1; Gaussian Inc.: Wallingford, CT, 2009.
(36) *TopSpin*, version 3.0; Bruker AXS: Madison, WI, 2010.
(37) Sandström, J. *Dynamic NMR Spectroscopy*; Academic Press: London, 1982.
(38) Witosińska, A.; Musielak, B.; Serda, P.; Owińska, M.; Rys, B. *J. Org. Chem.* **2012**, *77*, 9784−9794.
(39) Allen, F. H.; Bruno, I. J. *Acta Crystallogr., Sect. B: Struct. Sci.* **2010**, *66*, 380−386.
(40) Keith, T. A. *AIMAll*, version 11.10.16, 2011, aim.tkgristmill.com.
(41) Scheins, S.; Zheng, S.-L.; Benedict, J. B.; Coppens, P. *Acta Crystallogr., Sect. B: Struct. Sci.* **2010**, *66*, 366−372.

DOI: 10.1021/acs.inorgchem.5b01533
Inorg. Chem. 2015, 54, 8423−8435